Chinese Journal of Aeronautics, (2016), xxx(xx): xxx–xxx

Chinese Society of Aeronautics and Astronautics
& Beihang University

Chinese Journal of Aeronautics

cja@buaa.edu.cn
www.sciencedirect.com

A new steering approach for VSCMGs with high precision

Huang Xinghong, Jia Yinghong *, Xu Shijie, Huang Tingxuan

School of Astronautics, Beihang University, Beijing 100083, China

Received 9 September 2015; revised 17 October 2016; accepted 17 October 2016

KEYWORDS

Attitude control;
Dead-zone nonlinearity;
Integrated singularity measurement;
Singularity avoidance;
Variable speed control moment gyros (VSCMGs);
Wheel speed equalization

Abstract A new variable speed control moment gyro (VSCMG) steering law is proposed in order to achieve higher torque precision. The dynamics of VSCMGs is established, and two work modes are then designed according to command torque: control momentum gyro (CMG)/reaction wheel (RW) hybrid mode for the large torque case and RW single mode for the small. When working in the CMG/RW hybrid mode, the steering law deals with the gimbal dead-zone nonlinearity through compensation by RW sub-mode. This is in contrast to the conventional CMG singularity avoidance and wheel speed equalization, as well as the proof of definitely hyperbolic singular property of the CMG sub-mode. When working in the RW single mode, the motion of gimbals will be locked. Both the transition from CMG/RW hybrid mode to RW single mode and the reverse are studied. During the transition, wheel speed equalization and singularity avoidance of both the CMG and RW sub-modes are considered. A steering law for the RWs with locked gimbals is presented. It is shown by simulations that the VSCMGs with this new steering law could reach a better torque precision than the normal CMGs in the case of both large and small torques.

1. Introduction

Control momentum gyros (CMGs) have been used as spacecraft attitude control actuators for many years.[1–3] Due to their torque amplification feature, single-gimbal constant speed CMGs (CSCMGs) are especially advantageous for actuating large spacecraft and space structures,[4] or agile satellites that need rapid maneuverability.[5,6] Extensive testing results have been obtained for attitude control with CSCMGs (usually referred to as CMGs when there is no risk of confusion). Some of these focus on the subject of CMG configuration design, such as roof type,[7] and pyramid[8] or five pyramid type systems.[4,9] Margulies and Aubrun[10] and Bedrossian et al.[11] analyzed the corresponding singularities, and divided them into two types for which null motion[12] and robust pseudo-inverse method[13,14] are adopted to avoid/escape. In addition, Montfort and Dulot[15] investigated the reconfiguration of a CMG system in case of failures. Although CMGs can provide larger torque than reaction wheels (RWs), they also introduce larger torque error. To reduce this torque error, several approaches

* Corresponding author.
E-mail address: jia_yingh@163.com (Y. Jia).

Peer review under responsibility of Editorial Committee of CJA.

ELSEVIER Production and hosting by Elsevier

http://dx.doi.org/10.1016/j.cja.2016.10.017
1000-9361 © 2016 Production and hosting by Elsevier Ltd. on behalf of Chinese Society of Aeronautics and Astronautics.

have been proposed including to model the system as precisely as possible[16,17] or to utilize certain variation isolation methods.[18] A third is to employ mixed actuators for spacecraft attitude control.[19,20] The first two approaches, however, essentially cannot decrease torque error, and the third, despite of its ability to produce more precise torque, requires more than one set of actuators.

In 1997, Ford and Hall first introduced the concept of a variable speed control moment gyro (VSCMG) when it was called a "gimbaled momentum wheel."[21] The term VSCMG was coined in Ref. 22 Whereas the wheel speed of a conventional CMG is kept constant, the wheel speed of a VSCMG is allowed to vary continuously. Consequently, a VSCMG can be considered as an integration of a RW and a conventional CMG. The extra degrees of freedom, owing to wheel speed variance, can be used to avoid the singularities of its CMG sub-mode,[23,24] or store kinetic energy in an integrated power/attitude control system (IPACS).[25,26] When considering the lifespan and reliability of the actuators, wheel speed equalization is an extra issue for VSCMGs, and useful algorithms toward this objective have been developed.[27–29] However, the problem of reducing the torque error of VSCMGs by utilizing extra degrees of freedom has barely been explored.

In this paper, a new steering law is proposed for one set of VSCMGs that can provide high-precision torque outputs for both large and small command torque inputs by fully utilizing the two work modes of a VSCMG. The operation mechanism of the steering law is shown in Fig. 1. The remainder of this paper is organized as follows: Section 2 models the dynamics and divides the work modes of the VSCMGs. The steering law for CMG/RW hybrid mode and RW single mode are then designed in Sections 3 and 4. Section 5 presents numerical examples to verify the effectiveness of the proposed steering logic, and the paper closes with concluding remarks.

2. Dynamics and work modes of VSCMGs

A VSCMG is composed of a spin wheel and a gimbal that supports it, as shown in Fig. 2. The gimbal rotates about the gimbal axis, whose unit vector is denoted as $\boldsymbol{g}$, and the wheel rotates about the spin axis, whose unit vector is denoted as $\boldsymbol{s}$. $\boldsymbol{g}$ is perpendicular to $\boldsymbol{s}$. The angular velocities of the gimbal and the wheel are denoted as $\dot{\delta}$ and Ω, respectively, where δ is the gimbal angle of the VSCMG, and together they produce an angular momentum $\boldsymbol{h}$. The gimbal movement changes the direction of angular momentum, and thus generates torque by CMG sub-mode in the opposite direction of the unit vector $\boldsymbol{t}$, which is given as $\boldsymbol{g} \times \boldsymbol{s}$; variation of the wheel speed produces

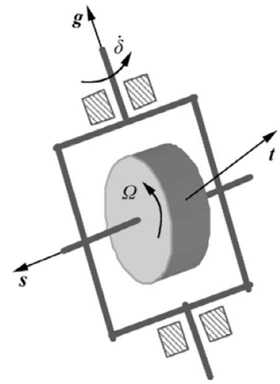

Fig. 2 Structure of a VSCMG.

torque by RW sub-mode in the direction of $\boldsymbol{s}$. Generally speaking, the torque of CMG sub-mode is far greater than that of RW, and the total output torque of the VSCMG is mainly from the CMG sub-mode. Therefore, the total torque of the VSCMG deviates slightly from the opposite direction of $\boldsymbol{t}$.

A cluster of VSCMGs is usually composed of n ($n \geqslant 3$) non-coplanar VSCMGs for three-axis attitude control of a spacecraft, and each VSCMG in the cluster usually holds the same mass and inertia parameters as another. Note that the pyramid and five pyramid configurations all belong to the non-coplanar type. In general, it is reasonable to consider only the axial angular momentum of the wheels.[22,24] Therefore, the total angular momentum of the VSCMGs can be expressed in the spacecraft body frame as

$$\boldsymbol{h}_{\mathrm{c}} = \sum_{i=1}^{n} \boldsymbol{h}_i = \sum_{i=1}^{n} I\Omega_i \boldsymbol{s}_i = \boldsymbol{A}_s I \boldsymbol{\Omega} \tag{1}$$

where $\boldsymbol{h}_i$ and Ω_i represent the axial angular momentum and the spin rate of the wheel of the ith VSCMG; I is the axial moment of inertia of each wheel in the cluster; $\boldsymbol{s}_i$ is the unit column vector for the ith VSCMG along the direction of the spin axis; $\boldsymbol{A}_s = [\boldsymbol{s}_1, \boldsymbol{s}_2, \ldots, \boldsymbol{s}_n]$; and $\boldsymbol{\Omega} = [\Omega_1, \Omega_2, \ldots, \Omega_n]^{\mathrm{T}}$.

According to theorem of angular momentum, the output torque of the VSCMGs can be given by the time derivative of $\boldsymbol{h}_{\mathrm{c}}$, that is

$$\begin{cases} \boldsymbol{T}_{\mathrm{c}} = -\dot{\boldsymbol{h}}_{\mathrm{c}} = -\boldsymbol{A}_t I[\boldsymbol{\Omega}]^{\mathrm{d}} \dot{\boldsymbol{\delta}} - \boldsymbol{A}_s I \dot{\boldsymbol{\Omega}} \\ \quad = \boldsymbol{C}(\boldsymbol{\delta}, \boldsymbol{\Omega}) \dot{\boldsymbol{\delta}} + \boldsymbol{D}(\boldsymbol{\delta}) \dot{\boldsymbol{\Omega}} \\ \boldsymbol{C}(\boldsymbol{\delta}, \boldsymbol{\Omega}) = -\boldsymbol{A}_t I[\boldsymbol{\Omega}]^{\mathrm{d}} \\ \boldsymbol{D}(\boldsymbol{\delta}) = -\boldsymbol{A}_s I \end{cases} \tag{2}$$

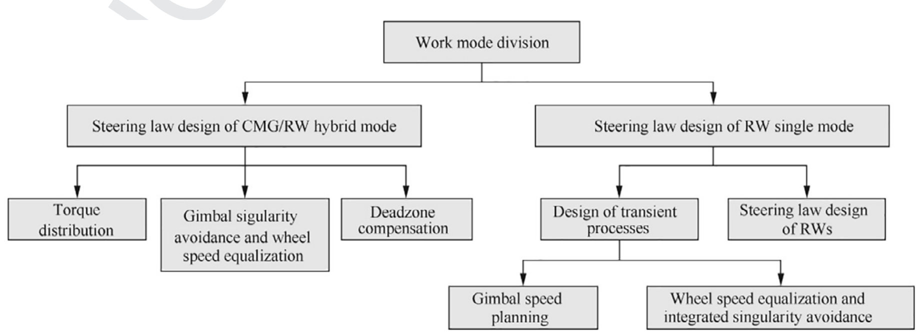

Fig. 1 A design flow chart of the high-precision steering law for VSCMGs.

Please cite this article in press as: Huang X et al. A new steering approach for VSCMGs with high precision, *Chin J Aeronaut* (2016), http://dx.doi.org/10.1016/j.cja.2016.10.017

where $\boldsymbol{A}_t = [\boldsymbol{t}_1, \boldsymbol{t}_2, \ldots, \boldsymbol{t}_n]$ in which $\boldsymbol{t}_i$ is the unit column vector for the ith VSCMG along the direction of the transverse axis; $\boldsymbol{\delta} = [\delta_1, \delta_2, \ldots, \delta_n]^{\mathrm{T}}$, with δ_i the gimbal angle of the ith VSCMG; and $[\cdot]^{\mathrm{d}}$ is an operator that brings an arbitrary column vector $\boldsymbol{z} = [z_1, z_2, \ldots, z_n]^{\mathrm{T}}$ to a diagonal matrix defined as

$$[\boldsymbol{z}]^{\mathrm{d}} = \mathrm{diag}(z_1, z_2, \ldots, z_n) \tag{3}$$

From Eq. (2) it can be seen that the output torque of the VSCMGs can be divided into two parts. The first part, $\boldsymbol{C}(\boldsymbol{\delta}, \boldsymbol{\Omega})\dot{\boldsymbol{\delta}}$, caused by the change of the direction of $\boldsymbol{h}_{\mathrm{c}}$, is called the CMG sub-mode. The second part, $\boldsymbol{D}(\boldsymbol{\delta})\dot{\boldsymbol{\Omega}}$, caused by the variation in magnitude of $\boldsymbol{h}_{\mathrm{c}}$, is called the RW sub-mode.

To calculate $\boldsymbol{A}_s$ and $\boldsymbol{A}_t$ in Eq. (2), we make the following deduction. The vectors $\boldsymbol{s}_i$ and $\boldsymbol{t}_i$ in $\boldsymbol{A}_s$ and $\boldsymbol{A}_t$ can be computed as

$$\boldsymbol{s}_i = \cos\delta_i \boldsymbol{s}_{i0} + \sin\delta_i \boldsymbol{t}_{i0} \tag{4}$$

$$\boldsymbol{t}_i = \cos\delta_i \boldsymbol{t}_{i0} - \sin\delta_i \boldsymbol{s}_{i0} \tag{5}$$

where $\boldsymbol{s}_{i0}$ and $\boldsymbol{t}_{i0}$ are the initial values of $\boldsymbol{s}_i$ and $\boldsymbol{t}_i$, respectively. Taking the time derivative of Eqs. (4) and (5) yields

$$\dot{\boldsymbol{s}}_i = \dot{\delta}_i \boldsymbol{t}_i, \qquad \dot{\boldsymbol{t}}_i = -\dot{\delta}_i \boldsymbol{s}_i \tag{6}$$

Consequently, $\boldsymbol{A}_s$ and $\boldsymbol{A}_t$, which are functions of gimbal angles, can be written as

$$\boldsymbol{A}_s = \boldsymbol{A}_{s0}[\cos\boldsymbol{\delta}]^{\mathrm{d}} + \boldsymbol{A}_{t0}[\sin\boldsymbol{\delta}]^{\mathrm{d}} \tag{7}$$

$$\boldsymbol{A}_t = \boldsymbol{A}_{t0}[\cos\boldsymbol{\delta}]^{\mathrm{d}} - \boldsymbol{A}_{s0}[\sin\boldsymbol{\delta}]^{\mathrm{d}} \tag{8}$$

where $\boldsymbol{A}_{s0}$ and $\boldsymbol{A}_{t0}$ are the initial values of $\boldsymbol{A}_s$ and $\boldsymbol{A}_v$, respectively; and $\sin\boldsymbol{\delta} = [\sin\delta_1, \sin\delta_2, \ldots, \sin\delta_n]^{\mathrm{T}}$, $\cos\boldsymbol{\delta} = [\cos\delta_1, \cos\delta_2, \ldots, \cos\delta_n]^{\mathrm{T}}$.

Denoting $\boldsymbol{R} = [\boldsymbol{C}, \boldsymbol{D}]$ and $\boldsymbol{x} = \begin{bmatrix} \dot{\boldsymbol{\delta}} \\ \dot{\boldsymbol{\Omega}} \end{bmatrix}$, Eq. (2) can also be written in the more compact form of

$$\boldsymbol{T}_{\mathrm{c}} = \boldsymbol{R}\boldsymbol{x} \tag{9}$$

The steering law for the VSCMGs is developed based on Eq. (9). The work mode of VSCMGs is first divided into two sub modes according to the magnitude of the command torque. One is the CMG/RW hybrid mode, which generates relatively large torque with motions of gimbals and wheels, and the other is the RW single mode, which generates high-precision small torque with the gimbals locked and only the wheels in motion. In the CMG/RW hybrid mode, torque error can increase due to the torque amplification feature of CMG sub-mode. In contrast, gimbals are locked in the RW single mode, and the torque error amplification effect vanishes, yielding higher output torque accuracy than the CMG/RW hybrid mode. The VSCMG system in RW single mode is essentially similar to a set of reaction wheels.

Considering the operating conditions of a spacecraft, it is suggested that a work mode switching strategy be applied based on the spacecraft flight mode, which can be obtained from control systems in orbit. In order to accommodate different application scenarios and maintain significant performance, a switching strategy for the two work modes is designed as follows: When performing an attitude maneuver, the VSCMG system is placed in the CMG/RW hybrid mode; once the maneuver is finished and the attitude is expected to be stable in the subsequent period, a "lock gimbals" command is relayed to the VSCMGs, and then a transient process of locking all the gimbals from CMG/RW hybrid mode to RW single mode is applied. When the gimbals are locked completely, the VSCMGs switch to the RW single mode. When a new attitude maneuver is required again, an "unlock gimbals" command will be sent to the VSCMGs, and, similarly, the VSCMGs will switch into a transient process of unlocking all the gimbals from RW single mode to the CMG/RW hybrid mode. Once the transition is completed, the VSCMGs work under CMG/RW hybrid mode and can provide the large torque required in fast attitude maneuvers.

In the next two sections, steering laws of CMG/RW hybrid mode and RW single mode are designed. The transient process of locking the gimbals from CMG/RW hybrid mode to the RW single mode and the reverse unlocking process are considered part of the RW single mode.

3. Steering law of CMG/RW hybrid mode

When large torque is needed, such as during attitude maneuvers, the VSCMG system is expected to work under the CMG/RW hybrid mode. For design of the hybrid mode steering law, firstly, a weighted pseudo-inverse solution $\boldsymbol{x}_{\mathrm{T}}$ and a null space solution $\boldsymbol{x}_{\mathrm{N}}$ of Eq. (9) are derived. The dead-zone nonlinearity of gimbal angular velocity is then compensated by the RW sub-mode, which can reduce torque error.

3.1. A weighted pseudo-inverse solution based on the singularity measurement for torque distribution

Because of the torque amplification function of the CMG sub-mode, the desired torque is expected to be supplied mainly by the CMG sub-mode when the gimbal configuration is far away from singular states. When the gimbal configuration is near singular states, the RW sub-mode is expected to provide more torque within its capability. According to this idea, a weighted pseudo-inverse solution for torque distribution based on the singularity measurement of Eq. (9) is achieved as[22,24]

$$\boldsymbol{x}_{\mathrm{T}} = \begin{bmatrix} \dot{\boldsymbol{\delta}}_{\mathrm{T}} \\ \dot{\boldsymbol{\Omega}}_{\mathrm{T}} \end{bmatrix} = \boldsymbol{R}_{\mathrm{w}}^{+}\boldsymbol{T}_{\mathrm{c}} \tag{10}$$

where $\boldsymbol{R}_{\mathrm{w}}^{+} = \boldsymbol{W}\boldsymbol{R}^{\mathrm{T}}(\boldsymbol{R}\boldsymbol{W}\boldsymbol{R}^{\mathrm{T}})^{-1}$ is a weighted pseudo-inverse of $\boldsymbol{R}$; the weight matrix $\boldsymbol{W}$ takes the form of $\boldsymbol{W} = \mathrm{diag}(W_{g1}, W_{g2}, \ldots, W_{gn}, W_{s1}, W_{s2}, \ldots, W_{sn})$, where $W_{gj} = 1$, $W_{sj} = W_{sj}^{0}\mathrm{e}^{-\varepsilon\kappa_1}$ for $j = 1, 2, \ldots, n$, in which $\kappa_1 = \det(\boldsymbol{A}_v\boldsymbol{A}_t^{\mathrm{T}})$ is the singularity measurement of the gimbal, and W_{sj}^{0} and ε are respective positive parameters that can be adjusted. The ratio between W_{gj} and W_{sj} reflects that between the torques supplied by CMG and RW sub-modes. That is, when the gimbal configuration is far away from singular states, κ_1 has a larger value, and W_{sj} is relatively small, yielding a relatively small torque by the RW sub-mode. Otherwise, a smaller κ_1 leads to a larger W_{sj}, and then larger torque will be contributed to the RW sub-mode.

From the weighted pseudo-inverse solution above, the gimbal angle velocities are

$$\dot{\boldsymbol{\delta}} = \boldsymbol{W}_1\boldsymbol{C}^{\mathrm{T}}(\boldsymbol{C}\boldsymbol{W}_1\boldsymbol{C}^{\mathrm{T}} + \boldsymbol{D}\boldsymbol{W}_2\boldsymbol{D}^{\mathrm{T}})^{-1}\boldsymbol{T}_{\mathrm{c}} \tag{11}$$

where $\boldsymbol{W}_1 = \mathrm{diag}(W_{g1}, W_{g2}, \ldots, W_{gn})$ and $\boldsymbol{W}_2 = \mathrm{diag}(W_{s1}, W_{s2}, \ldots, W_{sn})$ are weight sub-matrices of $\boldsymbol{W}$. Eq. (11) holds a similar mathematical form as the singularity robust steering law proposed by Wie[13]:

$$\dot{\boldsymbol{x}}_{\mathrm{c}} = \boldsymbol{W}_{\mathrm{c}}\boldsymbol{A}_{\mathrm{c}}^{\mathrm{T}}(\boldsymbol{A}_{\mathrm{c}}\boldsymbol{W}_{\mathrm{c}}\boldsymbol{A}^{\mathrm{T}} + \boldsymbol{V}_{\mathrm{c}})^{-1}\boldsymbol{\tau}_{\mathrm{c}} \tag{12}$$

where $\boldsymbol{x}_{\mathrm{c}}$, $\boldsymbol{W}_{\mathrm{c}}$, $\boldsymbol{A}_{\mathrm{c}}$, $\boldsymbol{V}_{\mathrm{c}}$ and $\boldsymbol{\tau}_{\mathrm{c}}$ represent gimbal angle, weight matrix, CMG torque matrix, supplementary robust term and desired torque, respectively. Comparing Eq. (11) with Eq. (12) we can see that the term $\boldsymbol{D}\boldsymbol{W}_2\boldsymbol{D}^{\mathrm{T}}$ in Eq. (11) plays a similar role as the term $\boldsymbol{V}_{\mathrm{c}}$ in Eq. (12), which implies that the weighted pseudo-inverse solution Eq. (10) has the capability of escaping from CMG singularities automatically to some extent. It is also noticeable that the steering law Eq. (12) was designed for CSCMGs, and it cannot be free from torque error; however, the weighted pseudo-inverse solution Eq. (10) does not produce any torque error with the aid of the extra RW sub-mode.

3.2. A null space solution for CMG singularity avoidance/escape and wheel speed equalization

It is well known that a cluster of VSCMGs with a non-coplanar configuration is theoretically always nonsingular; however, in practice the output torque is mainly presented by the CMG sub-mode, which is probably singular, and it is called the CMG singularity of the VSCMGs. Therefore, avoidance of the CMG singularity is of great significance. In addition, wheel speed equalization is also an important issue. Since the wheel speeds of the VSCMGs vary with time, the wheels may work at significantly different speeds for long periods, and this is harmful to the reliability and lifespan of the system. Hence, nearly equal speeds for all wheels are expected for an excellent steering law. Both CMG singularity avoidance and wheel speed equalization can be achieved by a null space solution that generates zero torque. In this section, the null space solution is derived, together with the proof for a theorem that shows the existence of the null space solution for all CMG singularities.

The corresponding homogeneous equation of Eq. (9) is

$$\boldsymbol{0} = \boldsymbol{R}\boldsymbol{x} \tag{13}$$

and a general solution of Eq. (13) is

$$\boldsymbol{x}_{\mathrm{N}} = k_{\mathrm{N}}\boldsymbol{P}_{\boldsymbol{R}}\boldsymbol{y} \tag{14}$$

where k_{N} is a constant scalar to be determined; $\boldsymbol{y}$ is an arbitrary $2n \times 1$ vector; $\boldsymbol{P}_{\boldsymbol{R}} = (\boldsymbol{E}_{2n} - \boldsymbol{R}_{\mathrm{w}}^{+}\boldsymbol{R})W$ is a positive semi-definite symmetric matrix, with $\boldsymbol{E}_{2n}$ the $2n$-order identity matrix. The Lyapunov method is used to design a vector $\boldsymbol{y}$ to achieve singularity avoidance and wheel speed equalization.

Let $\boldsymbol{\delta}_{\mathrm{f}}$ and $\boldsymbol{\Omega}_{\mathrm{f}}$ be the desired gimbal angle position and the desired wheel speed, respectively, then an error state variable can be defined by $\boldsymbol{e}_{\mathrm{a}} = \begin{bmatrix} \boldsymbol{\delta}_{\mathrm{f}} - \boldsymbol{\delta} \\ \boldsymbol{\Omega}_{\mathrm{f}} - \boldsymbol{\Omega} \end{bmatrix}$. Its time derivative is $\dot{\boldsymbol{e}}_{\mathrm{a}} = -(\boldsymbol{x}_{\mathrm{T}} + \boldsymbol{x}_{\mathrm{N}}) = -\boldsymbol{x}$. Selecting $V_{\mathrm{a}} = \frac{1}{2}\boldsymbol{e}_{\mathrm{a}}^{\mathrm{T}}\boldsymbol{e}_{\mathrm{a}} \geqslant 0$ as the Lyapunov function and using Eq. (14), the time derivative of V_{a} is

$$\dot{V}_{\mathrm{a}} = \boldsymbol{e}_{\mathrm{a}}^{\mathrm{T}}\dot{\boldsymbol{e}}_{\mathrm{a}} = -\boldsymbol{e}_{\mathrm{a}}^{\mathrm{T}}(\boldsymbol{x}_{\mathrm{T}} + \boldsymbol{x}_{\mathrm{N}}) = -\boldsymbol{e}_{\mathrm{a}}^{\mathrm{T}}\boldsymbol{x}_{\mathrm{T}} - k_{\mathrm{N}}\boldsymbol{e}_{\mathrm{a}}^{\mathrm{T}}\boldsymbol{P}_{\boldsymbol{R}}\boldsymbol{y} \tag{15}$$

Clearly, if $\boldsymbol{y}$ chosen as $\boldsymbol{y} = \boldsymbol{e}_{\mathrm{a}}$, $k_{\mathrm{N}}\boldsymbol{e}_{\mathrm{a}}^{\mathrm{T}}\boldsymbol{P}_{\boldsymbol{R}}\boldsymbol{y}$ takes its maximum positive value, $\dot{V}_{\mathrm{a}}$ becomes as small as possible. According to the Lyapunov theorem, the error variable $\boldsymbol{e}_{\mathrm{a}}$ is global asymptotically stable if the null space solution is given by

$$\begin{aligned} \boldsymbol{x}_{\mathrm{N}} &= k_{\mathrm{N}}\boldsymbol{P}_{\boldsymbol{R}}\boldsymbol{y} = k_{\mathrm{N}}\boldsymbol{P}_{\boldsymbol{R}}\boldsymbol{e}_{\mathrm{a}} \\ &= k_{\mathrm{N}}(\boldsymbol{E}_{2n} - \boldsymbol{R}_{\mathrm{w}}^{+}\boldsymbol{R})\boldsymbol{W}\begin{bmatrix} \boldsymbol{\delta}_{\mathrm{f}} - \boldsymbol{\delta} \\ \boldsymbol{\Omega}_{\mathrm{f}} - \boldsymbol{\Omega} \end{bmatrix} \end{aligned} \tag{16}$$

Next, the desired gimbal angle position $\boldsymbol{\delta}_{\mathrm{f}}$ and wheel speed $\boldsymbol{\Omega}_{\mathrm{f}}$ are computed. $\boldsymbol{\Omega}_{\mathrm{f}}$ can be chosen directly as the expected constant value of the wheel speed, but the choice of $\boldsymbol{\delta}_{\mathrm{f}}$ is much more complicated, as is shown below.

In order to obtain $\boldsymbol{\delta}_{\mathrm{f}}$, define $\Delta\boldsymbol{\delta} = \boldsymbol{\delta}_{\mathrm{f}} - \boldsymbol{\delta}$ as the gimbal angle error and $\kappa_2 = \frac{\sigma_3}{\sigma_1}$ as a second singularity measurement, where σ_{1v} and σ_{3t} are the maximum and minimum singular values of $\boldsymbol{A}_t$, respectively. Let $\kappa_2(\boldsymbol{\delta})$ and $\kappa_2(\boldsymbol{\delta} + \Delta\boldsymbol{\delta})$ denote the singularity measurement at times t and $t + \Delta t$, respectively, where Δt is a small time interval. By employing first order Taylor expansion we obtain

$$\kappa_2(\boldsymbol{\delta} + \Delta\boldsymbol{\delta}) = \kappa_2(\boldsymbol{\delta}) + \left(\frac{\partial\kappa_2}{\partial\boldsymbol{\delta}}\right)^{\mathrm{T}}\Delta\boldsymbol{\delta} \tag{17}$$

Notice that the range of κ_2 is $0 \leqslant \kappa_2 \leqslant 1$, and the further the gimbal position is away from singular states, the closer the singularity measurement κ_2 is to 1. Set $\kappa_2(\boldsymbol{\delta} + \Delta\boldsymbol{\delta})$ as the maximum value of 1, and substituting it into Eq. (17) we can get the minimum norm solution of $\Delta\boldsymbol{\delta}$ as

$$\Delta\boldsymbol{\delta} = \frac{\partial\kappa_2}{\partial\boldsymbol{\delta}}\left[\left(\frac{\partial\kappa_2}{\partial\boldsymbol{\delta}}\right)^{\mathrm{T}}\frac{\partial\kappa_2}{\partial\boldsymbol{\delta}}\right]^{-1}(1 - \kappa_2(\boldsymbol{\delta})) = \frac{1 - \kappa_2(\boldsymbol{\delta})}{|\partial\kappa_2/\partial\boldsymbol{\delta}|^2}\cdot\frac{\partial\kappa_2}{\partial\boldsymbol{\delta}} \tag{18}$$

where

$$\frac{\partial\kappa_2}{\partial\boldsymbol{\delta}} = -\frac{1}{\sigma_{1t}}\begin{bmatrix} \boldsymbol{u}_{3t}^{\mathrm{T}}\boldsymbol{s}_1 v_{13,t} \\ \boldsymbol{u}_{3t}^{\mathrm{T}}\boldsymbol{s}_2 v_{23,t} \\ \vdots \\ \boldsymbol{u}_{3t}^{\mathrm{T}}\boldsymbol{s}_n v_{n3,t} \end{bmatrix} + \frac{\sigma_{3t}}{\sigma_{1t}^2}\begin{bmatrix} \boldsymbol{u}_{1t}^{\mathrm{T}}\boldsymbol{s}_1 v_{11,t} \\ \boldsymbol{u}_{1t}^{\mathrm{T}}\boldsymbol{s}_2 v_{21,t} \\ \vdots \\ \boldsymbol{u}_{1t}^{\mathrm{T}}\boldsymbol{s}_n v_{n1,t} \end{bmatrix} \tag{19}$$

(for the deduction of Eq. (19), see Appendix A).

Using Eq. (18), the desired gimbal angle $\boldsymbol{\delta}_{\mathrm{f}}$ can be computed as $\boldsymbol{\delta}_{\mathrm{f}} = \boldsymbol{\delta} + \Delta\boldsymbol{\delta}$.

The preceding null space solution can be used for singularity avoidance and/or escape. The important concern then arises, like in the CSCMG system, of whether the null space solution always exists at a singular point or not. The type of singularity for CSCMGs is called elliptic when its null space solution does not exist and hyperbolic otherwise.[10,11] In contrast, as shown in the following theorem, the null space solution at any CMG singularity of VSCMGs always exists with the reconfiguration of not only gimbal angles $\boldsymbol{\delta}$, but also wheel speeds $\boldsymbol{\Omega}$.

Theorem 1. *All the internal CMG singularities of VSCMGs are hyperbolic, i.e. the null space solution at any CMG singularity always exists.*

Proof. Denote a CMG singularity by $\boldsymbol{x}^{\mathrm{s}} = \begin{bmatrix} \boldsymbol{\delta}^{\mathrm{s}} \\ \boldsymbol{\Omega}^{\mathrm{s}} \end{bmatrix}$, and the corresponding ith and total angular momentum by $\boldsymbol{h}_i^{\mathrm{s}}$ and $\boldsymbol{h}_{\mathrm{c}}^{\mathrm{s}}$. By means of a Taylor series expansion, one can deduce

$$\begin{aligned}\mathrm{d}\boldsymbol{h}_i &= \boldsymbol{h}_i(\boldsymbol{x}^{\mathrm{s}}+\mathrm{d}\boldsymbol{x})-\boldsymbol{h}_i(\boldsymbol{x}^{\mathrm{s}})\\ &= \sum_{k=1}^{+\infty}\frac{1}{k!}\left(\frac{\partial}{\partial\delta_i}\mathrm{d}\delta_i+\frac{\partial}{\partial\Omega_i}\mathrm{d}\Omega_i\right)^k\boldsymbol{h}_i\end{aligned} \tag{20}$$

In addition, the following relations can be derived from Eqs. (1) and (6):

$$\begin{cases}\frac{\partial\boldsymbol{h}_i}{\partial\delta_i}=\boldsymbol{t}_i|\boldsymbol{h}_i|,\quad \frac{\partial^2\boldsymbol{h}_i}{\partial^2\delta_i}=-\boldsymbol{h}_i,\quad \frac{\partial^3\boldsymbol{h}_i}{\partial^3\delta_i}=-\boldsymbol{t}_i|\boldsymbol{h}_i|,\quad \frac{\partial^4\boldsymbol{h}_i}{\partial^4\delta_i}=\boldsymbol{h}_i,\\ \frac{\partial^{\alpha+4}\boldsymbol{h}_i}{\partial^{\alpha+4}\delta_i}=\frac{\partial^{\alpha}\boldsymbol{h}_i}{\partial^{\alpha}\delta_i}\quad(\alpha\in\boldsymbol{N})\\ \frac{\partial^{\alpha+\beta}\boldsymbol{h}_i}{\partial^{\alpha}\delta_i\partial^{\beta}\Omega_i}=\boldsymbol{0}\quad(\alpha\in\{0\}\cup\mathbf{N},\beta\in\mathbf{N},\beta>1)\\ \frac{\partial\boldsymbol{h}_i}{\partial\Omega_i}=\boldsymbol{s}_iI,\quad \frac{\partial^2\boldsymbol{h}_i}{\partial\delta_i\partial\Omega_i}=\boldsymbol{t}_iI,\quad \frac{\partial^3\boldsymbol{h}_i}{\partial^2\delta_i\partial\Omega_i}=-\boldsymbol{s}_iI,\quad \frac{\partial^4\boldsymbol{h}_i}{\partial^3\delta_i\partial\Omega_i}=-\boldsymbol{t}_iI,\\ \frac{\partial^{\alpha+4}\boldsymbol{h}_i}{\partial^{\alpha+3}\delta_i\partial\Omega_i}=\frac{\partial^{\alpha}\boldsymbol{h}_i}{\partial^{\alpha-1}\delta_i\partial\Omega_i}\quad(\alpha\in\mathbf{N})\end{cases} \tag{21}$$

where $|\boldsymbol{h}_i| = I\Omega_i$ represents the magnitude of angular momentum $\boldsymbol{h}_i$. Substituting Eq. (21) into Eq. (20), we obtain

$$\begin{aligned}\mathrm{d}\boldsymbol{h}_i &= (\boldsymbol{t}_i|\boldsymbol{h}_i|\mathrm{d}\delta_i+\boldsymbol{s}_iI\mathrm{d}\Omega_i)+\frac{1}{2!}[-\boldsymbol{h}_i(\mathrm{d}\delta_i)^2+\boldsymbol{t}_iI\mathrm{d}\delta_i\mathrm{d}\Omega_i]\\ &\quad+\frac{1}{3!}[-\boldsymbol{t}_i|\boldsymbol{h}_i|(\mathrm{d}\delta_i)^3-\boldsymbol{s}_iI(\mathrm{d}\delta_i)^2\mathrm{d}\Omega_i]\\ &\quad+\frac{1}{4!}\left[\boldsymbol{h}_i(\mathrm{d}\delta_i)^4-\boldsymbol{t}_iI(\mathrm{d}\delta_i)^3\mathrm{d}\Omega_i\right]\\ &\quad+\frac{1}{5!}\left[\boldsymbol{t}_i|\boldsymbol{h}_i|(\mathrm{d}\delta_i)^5+\boldsymbol{s}_iI(\mathrm{d}\delta_i)^4\mathrm{d}\Omega_i\right]+\cdots\\ &= (\boldsymbol{t}_i|\boldsymbol{h}_i|\mathrm{d}\delta_i+\boldsymbol{s}_iI\mathrm{d}\Omega_i)\left[1-\frac{1}{3!}(\mathrm{d}\delta_i)^2+\frac{1}{5!}(\mathrm{d}\delta_i)^4-\dots\right]\\ &\quad+(\boldsymbol{h}_i\mathrm{d}\delta_i-\boldsymbol{t}_iI\mathrm{d}\Omega_i)\left[-\frac{1}{2!}\mathrm{d}\delta_i+\frac{1}{4!}(\mathrm{d}\delta_i)^3-\frac{1}{6!}(\mathrm{d}\delta_i)^5+\cdots\right]\end{aligned} \tag{22}$$

By virtue of power series expansion, we have

$$\begin{cases}1-\frac{1}{3!}(\mathrm{d}\delta_i)^2+\frac{1}{5!}(\mathrm{d}\delta_i)^4-\cdots=\frac{\sin(\mathrm{d}\delta_i)}{\mathrm{d}\delta_i}\\ -\frac{1}{2!}\mathrm{d}\delta_i+\frac{1}{4!}(\mathrm{d}\delta_i)^3-\frac{1}{6!}(\mathrm{d}\delta_i)^5+\cdots=\frac{1-\cos(\mathrm{d}\delta_i)}{\mathrm{d}\delta_i}\end{cases} \tag{23}$$

When $\mathrm{d}\delta_i\to 0$, $\frac{\sin(\mathrm{d}\delta_i)}{\mathrm{d}\delta_i}\to 1$, $\frac{1-\cos(\mathrm{d}\delta_i)}{\mathrm{d}\delta_i}\to\frac{\mathrm{d}\delta_i}{2}$. By substituting these into Eq. (22), we have

$$\mathrm{d}\boldsymbol{h}_i = (\boldsymbol{t}_i|\boldsymbol{h}_i|\mathrm{d}\delta_i+\boldsymbol{s}_iI\mathrm{d}\Omega_i)+\frac{1}{2}(\boldsymbol{h}_i\mathrm{d}\delta_i-\boldsymbol{t}_iI\mathrm{d}\Omega_i)\mathrm{d}\delta_i \tag{24}$$

which can be used to show that

$$\begin{aligned}\mathrm{d}\boldsymbol{h}_{\mathrm{c}} &= \sum_{i=1}^{n}\mathrm{d}\boldsymbol{h}_i\\ &= -(\boldsymbol{C}\mathrm{d}\boldsymbol{\delta}+\boldsymbol{D}\mathrm{d}\boldsymbol{\Omega})+\frac{1}{2}\sum_{i=1}^{n}[\boldsymbol{h}_i(\mathrm{d}\delta_i)^2-\boldsymbol{t}_iI\mathrm{d}\delta_i\mathrm{d}\Omega_i]\end{aligned} \tag{25}$$

When the CMG sub-mode of the VSCMGs is singular, the following constraints hold:

$$\boldsymbol{u}\cdot\boldsymbol{t}_i=0\quad(i=1,2,\dots,n) \tag{26}$$

where $\boldsymbol{u}$ represents the singular direction. With Eq. (26) and the equation $\boldsymbol{C}\mathrm{d}\boldsymbol{\delta}+\boldsymbol{D}\mathrm{d}\boldsymbol{\Omega}=\boldsymbol{0}$, since $\mathrm{d}\boldsymbol{x}=\begin{bmatrix}\mathrm{d}\boldsymbol{\delta}\\ \mathrm{d}\boldsymbol{\Omega}\end{bmatrix}$ is null motion, taking the dot product of Eq. (25) with $\boldsymbol{u}$ results in

$$\boldsymbol{u}\mathrm{d}\boldsymbol{h}_c=\frac{1}{2}\sum_{i=1}^{n}\boldsymbol{u}\boldsymbol{h}_i(\mathrm{d}\delta_i)^2=\frac{1}{2}\mathrm{d}\boldsymbol{\delta}^{\mathrm{T}}\boldsymbol{P}\mathrm{d}\boldsymbol{\delta} \tag{27}$$

where $\boldsymbol{P}=[p_1,p_2,\dots,p_n]^{\mathrm{d}}=[\boldsymbol{u}\boldsymbol{h}_1,\boldsymbol{u}\boldsymbol{h}_2,\dots,\boldsymbol{u}\boldsymbol{h}_n]^{\mathrm{d}}$. The definition of null motion implies $\mathrm{d}\boldsymbol{h}_{\mathrm{c}}\equiv\boldsymbol{0}$, and thus Eq. (27) becomes

$$\mathrm{d}\boldsymbol{\delta}^{\mathrm{T}}\boldsymbol{P}\mathrm{d}\boldsymbol{\delta}=0 \tag{28}$$

To obtain a null displacement solution for $\mathrm{d}\boldsymbol{\delta}$, express the overall null variations $\mathrm{d}\boldsymbol{x}$ as a linear combination of its null space basis vectors based on Eq. (13):

$$\begin{bmatrix}\mathrm{d}\boldsymbol{\delta}\\ \mathrm{d}\boldsymbol{\Omega}\end{bmatrix}=\mathrm{d}\boldsymbol{x}=\sum_{i=1}^{2n-\mathrm{rank}(\boldsymbol{R})}\lambda_i\boldsymbol{n}_i=\boldsymbol{N}\boldsymbol{\lambda}=\begin{bmatrix}\boldsymbol{N}_{\delta}\\ \boldsymbol{N}_{\Omega}\end{bmatrix}\boldsymbol{\lambda} \tag{29}$$

where $\boldsymbol{\lambda}=[\lambda_1,\lambda_2,\dots,\lambda_{2n-\mathrm{rank}(\boldsymbol{R})}]^{\mathrm{T}}$ is weight vector; $\boldsymbol{N}=[\boldsymbol{n}_1,\boldsymbol{n}_2,\dots,\boldsymbol{n}_{2n-\mathrm{rank}(\boldsymbol{R})}]^{\mathrm{T}}$ are null space basis vectors, with $\boldsymbol{N}_{\delta}$ and $\boldsymbol{N}_{\Omega}$ the top and bottom half sub-matrices of $\boldsymbol{N}$, respectively, both with the dimension $n\times(2n-\mathrm{rank}(\boldsymbol{R}))$. Note that for a non-coplanar VSCMG system, we have $\mathrm{rank}(\boldsymbol{R})=3$ and $2n-\mathrm{rank}(\boldsymbol{R})=2n-3>n$. From Eq. (29) we obtain

$$\mathrm{d}\boldsymbol{\delta}=\boldsymbol{N}_{\delta}\boldsymbol{\lambda} \tag{30}$$

Substituting it into Eq. (28) produces

$$\boldsymbol{\lambda}^{\mathrm{T}}\boldsymbol{Q}\boldsymbol{\lambda}=0 \tag{31}$$

where $\boldsymbol{Q}=\boldsymbol{N}_{\delta}^{\mathrm{T}}\boldsymbol{P}\boldsymbol{N}_{\delta}$. This quadratic form represents a constraint equation that the admissible null motions must satisfy in the vicinity of a singular point. For any $\boldsymbol{\lambda}$ satisfying Eq. (31), a null motion can be obtained by substituting it into Eq. (29).

Similarly to CSCMGs, the solutions to Eq. (31) can be classified according to the properties of the quadratic form as (i) definite $\boldsymbol{Q}$ or (ii) indefinite or singular $\boldsymbol{Q}$. When condition (i) holds, the only solution to Eq. (31) is $\boldsymbol{\lambda}=\boldsymbol{0}$, which indicates that this singular point is an isolated point and null motion is impossible; thus escape by null motion is impossible from this type of singular configuration. This type of singularity can be also termed elliptic. The other possibility for $\boldsymbol{Q}$ is to be indefinite or singular. This type of singularity can be termed hyperbolic. A nonzero solution about $\boldsymbol{\lambda}$ implies that null motion can be generated at the singularity, which generally guarantees escape from that singular point.

As a fact, $\boldsymbol{Q}$ is definitely singular for VSCMGs, which demonstrates that all internal CMG singularities are hyperbolic. By means of singular value decomposition, $\mathbf{N}_{\boldsymbol{\delta}}$ is given by

$$\begin{aligned}\boldsymbol{N}_{\delta}&=\boldsymbol{U}_{\delta}\boldsymbol{S}_{\delta}\boldsymbol{V}_{\delta}\\ &=[\boldsymbol{u}_{1\delta},\boldsymbol{u}_{2\delta},\dots,\boldsymbol{u}_{n\delta}]\begin{bmatrix}\sigma_{1\delta} & & \\ & \ddots & 0_{n\times(n-3)}\\ & \sigma_{n\delta} & \end{bmatrix}\begin{bmatrix}\boldsymbol{v}_{1\delta}^{\mathrm{T}}\\ \boldsymbol{v}_{2\delta}^{\mathrm{T}}\\ \vdots\\ \boldsymbol{v}_{(2n-3)\delta}^{\mathrm{T}}\end{bmatrix}\end{aligned} \tag{32}$$

Please cite this article in press as: Huang X et al. A new steering approach for VSCMGs with high precision, *Chin J Aeronaut* (2016), http://dx.doi.org/10.1016/j.cja.2016.10.017

where $\sigma_{i\delta}$ $(i = 1, 2, \ldots, n)$ are the singular values of $\boldsymbol{N}_\delta$, and $\boldsymbol{u}_{i\delta}$, $\boldsymbol{v}_{i\delta}$ the column vectors of $\boldsymbol{U}_\delta$ and $\boldsymbol{V}_\delta$, respectively. As a result, one can obtain

$$\boldsymbol{Q} = \boldsymbol{N}_\delta^{\mathrm{T}}\boldsymbol{P}\boldsymbol{N}_\delta = [\boldsymbol{v}_{1\delta}, \boldsymbol{v}_{2\delta}, \ldots, \boldsymbol{v}_{n\delta}]\begin{bmatrix} \sigma_{1\delta} & & \\ & \ddots & \\ & & \sigma_{n\delta} \\ 0_{(n-3)\times n} & & \end{bmatrix}\begin{bmatrix} \boldsymbol{u}_{1\delta}^{\mathrm{T}} \\ \boldsymbol{u}_{2\delta}^{\mathrm{T}} \\ \vdots \\ \boldsymbol{u}_{(2n-3)\delta}^{\mathrm{T}} \end{bmatrix} \times \begin{bmatrix} p_1 & & \\ & \ddots & \\ & & p_n \end{bmatrix} \cdot [\boldsymbol{u}_{1\delta}, \boldsymbol{u}_{2\delta}, \ldots, \boldsymbol{u}_{n\delta}]\begin{bmatrix} \sigma_{1\delta} & & & \\ & \ddots & & \boldsymbol{0}_{n\times(n-3)} \\ & & \sigma_{n\delta} & \end{bmatrix} \times \begin{bmatrix} \boldsymbol{v}_{1\delta}^{\mathrm{T}} \\ \boldsymbol{v}_{2\delta}^{\mathrm{T}} \\ \vdots \\ \boldsymbol{v}_{(2n-3)\delta}^{\mathrm{T}} \end{bmatrix} = \sum_{i=1}^{n}\eta \boldsymbol{v}_{i\delta}\boldsymbol{v}_{i\delta}^{\mathrm{T}} \tag{33}$$

where $\eta = p_1\sigma_{i\delta}^2$. Eq. (33) illustrates that $\mathrm{rank}(\boldsymbol{Q}) \leqslant n$, and, taking the relationship $n > 3$ into consideration, we obtain

$$\mathrm{rank}(\boldsymbol{Q}) \leqslant n < 2n - 3 \tag{34}$$

Since the dimension of $\boldsymbol{Q}$ is $(2n - 3) \times (2n - 3)$, $\boldsymbol{Q}$ is singular and implies that all the CMG singularities of the VSCMGs are hyperbolic. This completes the proof. □

3.3. A strategy of compensating the dead-zone nonlinearity of gimbal speeds

The dead-zone nonlinearity of rotational motion is one of the important problems that decrease servo control accuracy. When the rotation speed is within the dead-zone, the control accuracy will deteriorate rapidly due to friction. Furthermore, because of the torque amplification effect, for VSCMGs, the dead-zone nonlinearity of gimbal speeds is much more significant than that of wheel speeds. Therefore, an attempt is made here to improve the dead-zone nonlinearity of gimbal rotation speeds.

Recall that $\dot{\boldsymbol{\delta}} = \dot{\boldsymbol{\delta}}_{\mathrm{T}} + \dot{\boldsymbol{\delta}}_{\mathrm{N}}$, where $\dot{\boldsymbol{\delta}}_{\mathrm{T}}$ produces output torque while $\dot{\boldsymbol{\delta}}_{\mathrm{N}}$ is devoted to singularity avoidance. In order to mitigate the dead-zone effect, an scheme is designed to properly adjust $\dot{\boldsymbol{\delta}}_{\mathrm{T}}$.

Suppose the threshold of the dead-zone is $\dot{\delta}_{\min}$. If the ith gimbal rotation speed falls into the dead-zone, i.e. $|\dot{\delta}_i| < \dot{\delta}_{\min}$, we can adjust the solution $\dot{\delta}_{i\mathrm{T}}$ to $\dot{\delta}_{i\mathrm{T}} + \Delta\dot{\delta}_{i\mathrm{T}}$ along its previous rotational direction, which makes a new gimbal speed $\dot{\delta}_i^*$ out of the dead-zone $\dot{\delta}_{\min}$. That is to say, we get a new gimbal speed $\dot{\delta}_i^*$ such that

$$\begin{aligned} |\dot{\delta}_i^*| &= |(\dot{\delta}_{i\mathrm{T}} + \Delta\dot{\delta}_{i\mathrm{T}}) + \dot{\delta}_{i\mathrm{N}}| = |(\dot{\delta}_{i\mathrm{T}} + \dot{\delta}_{i\mathrm{N}}) + \Delta\dot{\delta}_{i\mathrm{T}}| \\ &= |\dot{\delta}_i + \Delta\dot{\delta}_{i\mathrm{T}}| \geqslant \dot{\delta}_{\min} \end{aligned} \tag{35}$$

As the increment $\Delta\dot{\delta}_{i\mathrm{T}}$ is along the same direction of $\dot{\delta}_{i\mathrm{T}}$, an adjusting algorithm can be given by

$$\Delta\dot{\delta}_{i\mathrm{T}} = \begin{cases} \mathrm{sign}(\dot{\delta}_i)|\dot{\delta}_{\min} - |\dot{\delta}_i|| & |\dot{\delta}_i| < \dot{\delta}_{\min} \\ 0 & |\dot{\delta}_i| \geqslant \dot{\delta}_{\min} \end{cases} \tag{36}$$

Note that $\Delta\dot{\delta}_{i\mathrm{T}}$ induces an error torque, which can be computed as

$$\Delta\boldsymbol{T} = -\boldsymbol{A}_t I[\boldsymbol{\Omega}]^{\mathrm{d}}\Delta\dot{\delta}_{i\mathrm{T}} \tag{37}$$

This error torque can be compensated by the RW sub-mode

$$\Delta\dot{\boldsymbol{\Omega}} = I^{-1}\boldsymbol{A}_s^{\mathrm{T}}\left(\boldsymbol{A}_s\boldsymbol{A}_s^{\mathrm{T}}\right)^{-1}\Delta\boldsymbol{T} \tag{38}$$

The resulting new wheel acceleration is

$$\dot{\boldsymbol{\Omega}}^* = \dot{\boldsymbol{\Omega}} + \Delta\dot{\boldsymbol{\Omega}} \tag{39}$$

Since the magnitude of $\Delta\dot{\delta}_{i\mathrm{T}}$ is below the dead-zone $\dot{\delta}_{\min}$, $\Delta\dot{\delta}_{i\mathrm{T}}$ and thus $\Delta\boldsymbol{T}$ takes small values. This feature ensures that torque error compensation is feasible by the RW sub-mode.

4. Steering law of RW single mode

When small torque is required, such as in attitude stabilization, VSCMGs are expected to work in the RW single mode. To this end, a steering law for this mode, including a switching process between the CMG/RW hybrid mode and the RW single mode, is designed in this section.

4.1. Two transient processes

The RW single mode can be considered as a special case of the CMG/RW hybrid mode in which the gimbals are locked. In this section, the process of locking the gimbals is designed as a transient process by the following two steps.

4.1.1. Gimbal speed planning of the transient process

The goal of the locking transient process is to reduce the gimbal speed to zero smoothly and, at the same time, maintain the desired output torque. Based on the former sections, the gimbal speed $\dot{\boldsymbol{\delta}}$ is composed of a weighted pseudo-inverse solution $\dot{\boldsymbol{\delta}}_{\mathrm{T}}$ that generates a nonzero torque and a null space solution $\dot{\boldsymbol{\delta}}_{\mathrm{N}}$ that generates a zero torque. This leads to the gimbal speed planning method of the transient process, which is to reduce the $\dot{\boldsymbol{\delta}}_{\mathrm{T}}$ and $\dot{\boldsymbol{\delta}}_{\mathrm{N}}$ to zeros synchronously.

The planning of $\dot{\boldsymbol{\delta}}_{\mathrm{T}}$ can be realized by planning its weight matrix $\boldsymbol{W}$; specifically, we design W_{gi} in $\boldsymbol{W} = \mathrm{diag}(W_{g1}, W_{g2}, \ldots, W_{gn}, W_{s1}, W_{s2}, \ldots, W_{sn})$ to be the following declining parabolic function

$$W_{gi} = \frac{W_{gi}^0}{T_{\mathrm{tr}}^2}(t - T_{\mathrm{tr}})^2 \quad i = 1, 2, \ldots, n \tag{40}$$

where t is current time from the beginning of the transient process; W_{gi}^0 is the initial value of W_{gi}; and T_{tr} is the time span of the transient process. The decrease of W_{gi} will produce a torque error $\Delta\boldsymbol{T}$, and this can be compensated via the RW sub-mode by adding $\Delta\dot{\boldsymbol{\Omega}}$ to the original wheel acceleration $\dot{\boldsymbol{\Omega}}$ where $\Delta\dot{\boldsymbol{\Omega}}$ is given by

$$\Delta\dot{\boldsymbol{\Omega}} = I^{-1}\boldsymbol{A}_s^{\mathrm{T}}\left(\boldsymbol{A}_s\boldsymbol{A}_s^{\mathrm{T}}\right)^{-1}\Delta\boldsymbol{T} \tag{41}$$

The planning of $\dot{\boldsymbol{\delta}}_{\mathrm{N}}$ can be realized by planning the coefficient k_{N} of the whole null space solution $\boldsymbol{x}_{\mathrm{N}} = k_{\mathrm{N}}\boldsymbol{P}_R\boldsymbol{y}$. k_{N} is also defined as a declining parabolic function:

$$k_{\mathrm{N}} = \frac{k_{\mathrm{N}}^{0}}{T_{\mathrm{tr}}^{2}}(t - T_{\mathrm{tr}})^{2} \tag{42}$$

where k_{N}^{0} is the initial value of k_{N}. Since the output torque of the null space solution is zero, the adjustment of k_{N} does not introduce any torque error.

4.1.2. A null space solution for integrated singularity avoidance and wheel speed equalization during transient process

There are three goals of this null space solution: singularity avoidance of the gimbals, singularity avoidance of the wheels, and wheel speed equalization. Compared with the second step in the last section, the only difference is that the additional goal for singularity avoidance of wheels is demanded here. Therefore, the method to get a null space solution here could be similar to that of the last section. The variation is only that the singularity measurement of the gimbals be replaced by an integrated singularity measurement $\kappa_{2,\mathrm{all}}$, which reflects the singular status for both the gimbals and the wheels, and is defined by

$$\kappa_{2,\mathrm{all}} = \kappa_{2,\mathrm{cmg}} \times \kappa_{2,\mathrm{rw}} \tag{43}$$

where $\kappa_{2,\mathrm{cmg}}$ is the second singularity measurement of the gimbals, which is just the former κ_{2}; and $\kappa_{2,\mathrm{rw}}$ is that of the wheels. $\kappa_{2,\mathrm{rw}}$ can be defined by $\kappa_{2,\mathrm{rw}} = \frac{\sigma_{3s}}{\sigma_{1s}}$, where σ_{1s} and σ_{3s} are the maximum and minimum singular values of $\boldsymbol{A}_s$, respectively, which reflect wheel configuration. It should be noted that both $\kappa_{2,\mathrm{cmg}}$ and $\kappa_{2,\mathrm{rw}}$ range from 0 to 1. The further the corresponding configuration is from singular states, the more the measurement is close to 1. So, if we set the expected integrated singularity measurement as $\kappa_{2,\mathrm{all}} = \kappa_{2,\mathrm{cmg}} \times \kappa_{2,\mathrm{rw}} = 1$, we can have $\kappa_{2,\mathrm{cmg}} = 1$ and $\kappa_{2,\mathrm{rw}} = 1$. Thus, both the gimbals and wheels will be far away from their singular states. For the integrated singularity measurement $\kappa_{2,\mathrm{all}}$, $\frac{\partial \kappa_{2,\mathrm{all}}}{\partial \boldsymbol{\delta}}$ can be computed as follows:

Supposing that the singular value decomposition of $\boldsymbol{A}_t$ is given by

$$\boldsymbol{A}_t = \boldsymbol{U}_t \boldsymbol{S}_t \boldsymbol{V}_t^{\mathrm{T}} = \sum_{i=1}^{3} \sigma_{it} \boldsymbol{u}_{it} \boldsymbol{v}_{it}^{\mathrm{T}} \tag{44}$$

We can obtain

$$\frac{\partial \kappa_{2,\mathrm{cmg}}}{\partial \boldsymbol{\delta}} = -\frac{1}{\sigma_{1t}} \begin{bmatrix} \boldsymbol{u}_{3t}^{\mathrm{T}} \boldsymbol{s}_1 v_{13,t} \\ \boldsymbol{u}_{3t}^{\mathrm{T}} \boldsymbol{s}_2 v_{23,t} \\ \vdots \\ \boldsymbol{u}_{3t}^{\mathrm{T}} \boldsymbol{s}_n v_{n3,t} \end{bmatrix} + \frac{\sigma_{3t}}{\sigma_{1t}^{2}} \begin{bmatrix} \boldsymbol{u}_{1t}^{\mathrm{T}} \boldsymbol{s}_1 v_{11,t} \\ \boldsymbol{u}_{1t}^{\mathrm{T}} \boldsymbol{s}_2 v_{21,t} \\ \vdots \\ \boldsymbol{u}_{1t}^{\mathrm{T}} \boldsymbol{s}_n v_{n1,t} \end{bmatrix} \tag{45}$$

Similarly, supposing the singular value decomposition of $\boldsymbol{A}_s$ is given by

$$\boldsymbol{A}_s = \boldsymbol{U}_s \boldsymbol{S}_s \boldsymbol{V}_s^{\mathrm{T}} = \sum_{i=1}^{3} \sigma_{is} \boldsymbol{u}_{is} \boldsymbol{v}_{is}^{\mathrm{T}} \tag{46}$$

where σ_{is} $(i = 1, 2, 3)$ are the singular values of $\boldsymbol{A}_s$, and $\boldsymbol{u}_{is}$, $\boldsymbol{v}_{is}$ the column vectors of $\boldsymbol{U}_s$ and $\boldsymbol{V}_s$, respectively. We then obtain

$$\frac{\partial \kappa_{2,\mathrm{rw}}}{\partial \boldsymbol{\delta}} = \frac{1}{\sigma_{1s}} \begin{bmatrix} \boldsymbol{u}_{3s}^{\mathrm{T}} \boldsymbol{t}_1 v_{13,s} \\ \boldsymbol{u}_{3s}^{\mathrm{T}} \boldsymbol{t}_2 v_{23,s} \\ \vdots \\ \boldsymbol{u}_{3s}^{\mathrm{T}} \boldsymbol{t}_n v_{n3,s} \end{bmatrix} - \frac{\sigma_{3s}}{\sigma_{1s}^{2}} \begin{bmatrix} \boldsymbol{u}_{1s}^{\mathrm{T}} \boldsymbol{t}_1 v_{11,s} \\ \boldsymbol{u}_{1s}^{\mathrm{T}} \boldsymbol{t}_2 v_{21,s} \\ \vdots \\ \boldsymbol{u}_{1s}^{\mathrm{T}} \boldsymbol{t}_n v_{n1,s} \end{bmatrix} \tag{47}$$

where $v_{ij,s}$ are the elements of vector $\boldsymbol{v}_{is}$. Finally, the result of $\frac{\partial \kappa_{2,\mathrm{all}}}{\partial \boldsymbol{\delta}}$ can be expressed as

$$\frac{\partial \kappa_{2,\mathrm{all}}}{\partial \boldsymbol{\delta}} = \frac{\partial(\kappa_{2,\mathrm{cmg}} \kappa_{2,\mathrm{rw}})}{\partial \boldsymbol{\delta}} = \frac{\partial(\kappa_{2,\mathrm{cmg}})}{\partial \boldsymbol{\delta}} \kappa_{2,\mathrm{rw}} + \kappa_{2,\mathrm{cmg}} \frac{\partial(\kappa_{2,\mathrm{rw}})}{\partial \boldsymbol{\delta}} \tag{48}$$

The transient process of unlocking the gimbals from the RW single mode to the CMG/RW hybrid mode is just the reverse process of locking the gimbals described above, so its planning work can be carried out similarly.

4.2. A steering law of RWs with gimbals locked completely

When the gimbals are completely locked, the VSCMGs have been turned into RWs, and it is essentially the same as general reaction wheel configurations. As long as the wheel configuration is nonsingular, which can be guaranteed by the transient process design, and wheel speeds are absent from saturation, three independent control torques can always be generated. A pseudo-inverse steering law can be designed as

$$\dot{\boldsymbol{\Omega}} = -I^{-1} \boldsymbol{A}_s^{\mathrm{T}} (\boldsymbol{A}_s \boldsymbol{A}_s^{T})^{-1} \boldsymbol{T}_{\mathrm{c}} \tag{49}$$

5. Numerical simulations

Numerical simulations are presented in this section to study the performance of the proposed steering law for VSCMGs. Attitude maneuvering/stabilization of a spacecraft is involved. Rigid spacecraft dynamics and the proportional-derivative (PD) controller deduced in Ref. 14 are applied here. We rewrite them here with slight symbol changes for convenience:

$$\boldsymbol{J}\dot{\boldsymbol{\omega}} + \dot{\boldsymbol{J}}\boldsymbol{\omega} + \boldsymbol{\omega}^{\times}(\boldsymbol{J}\boldsymbol{\omega} + \boldsymbol{A}_s \boldsymbol{I}\boldsymbol{\Omega}) = \boldsymbol{T}_{\mathrm{c}} \tag{50}$$

$$\begin{cases} \boldsymbol{T}_{\mathrm{c}} = [T_{\mathrm{c}x}, T_{\mathrm{c}y}, T_{\mathrm{c}z}]^{\mathrm{T}} \\ T_{\mathrm{c}x} = K_{\mathrm{p}x} e_{\phi} + K_{\mathrm{d}x} \dot{e}_{\phi} + \omega_{\mathrm{o}}(I_y - I_x - I_z)\dot{\psi} - h_{\mathrm{c}z}\omega_{\mathrm{o}} \\ T_{\mathrm{c}y} = K_{\mathrm{p}y} e_{\theta} + K_{\mathrm{d}y} \dot{e}_{\theta} \\ T_{\mathrm{c}z} = K_{\mathrm{p}z} e_{\psi} + K_{\mathrm{d}z} \dot{e}_{\psi} + \omega_{\mathrm{o}}(I_x + I_z - I_y)\dot{\phi} + h_{\mathrm{c}x}\omega_{\mathrm{o}} \end{cases} \tag{51}$$

where $\boldsymbol{\omega}$ is the attitude angle velocity of the spacecraft; ω_{o} is the magnitude of the orbit angle velocity; $e_{\phi} = \phi_{\mathrm{r}} - \phi$, $e_{\theta} = \theta_{\mathrm{r}} - \theta$ and $e_{\psi} = \psi_{\mathrm{r}} - \psi$ are attitude errors of the three axes between the actual Euler angles (ϕ, θ, ψ) and the expected final Euler angles $(\phi_{\mathrm{r}}, \theta_{\mathrm{r}}, \psi_{\mathrm{r}})$; $\boldsymbol{J} = \boldsymbol{I}_{\mathrm{o}} + \boldsymbol{A}_g \boldsymbol{I}_g \boldsymbol{A}_g^{\mathrm{T}} + \boldsymbol{A}_s \boldsymbol{I}_s \boldsymbol{A}_s^{\mathrm{T}} + \boldsymbol{A}_t \boldsymbol{I}_t \boldsymbol{A}_t^{\mathrm{T}}$ is the inertia of the total system, with $\boldsymbol{I}_{\mathrm{o}}$ the inertia of the spacecraft without VSCMGs, $\boldsymbol{I}_g = \mathrm{diag}(I_{g1}, I_{g2}, \ldots, I_{gn})$, $\boldsymbol{I}_s = \mathrm{diag}(I_{s1}, I_{s2}, \ldots, I_{sn})$, $\boldsymbol{I}_t = \mathrm{diag}(I_{t1}, I_{t2}, \ldots, I_{tn})$, and $I_{g,i}$, $I_{s,i}$ and $I_{t,i}$ $(i = 1, 2, \ldots, n)$ the moments of inertia along $\boldsymbol{g}$, $\boldsymbol{s}$ and $\boldsymbol{t}$ of the ith VSCMG, respectively, and $\boldsymbol{A}_g = [\boldsymbol{g}_1, \boldsymbol{g}_2, \ldots, \boldsymbol{g}_n]$; I_x, I_y and I_z are the diagonal elements of $\boldsymbol{J}$, which mean the principal axial moments of inertia; $h_{\mathrm{c}x}$ and $h_{\mathrm{c}z}$ are x and z components of the momentum of the total system, which can be computed as $\boldsymbol{H} = \boldsymbol{J}\boldsymbol{\omega}$; $K_{\mathrm{p}x}$, $K_{\mathrm{p}y}$, $K_{\mathrm{p}z}$ and $K_{\mathrm{d}x}$, $K_{\mathrm{d}y}$, $K_{\mathrm{d}z}$ are PD parameters of the PD controller.

The main parameters of the spacecraft-VSCMGs system used in the simulations are shown in Table 1, where $\Omega_{\min}$ and $\Omega_{\max}$ are the minimum and maximum values of wheel speed of a VSCMG; Ω_0 is Nominal wheel speed of a VSCMG; $\dot{\delta}_{\min}$ and $\dot{\delta}_{\max}$ are the minimum and maximum values of gimbal rotational speed of a VSCMG; $\boldsymbol{\delta}_0$ is the initial gimbal angles of the VSCMGs. These parameters are close to those of the

Please cite this article in press as: Huang X et al. A new steering approach for VSCMGs with high precision, *Chin J Aeronaut* (2016), http://dx.doi.org/10.1016/j.cja.2016.10.017

Table 1 System model parameters and initial conditions.

Variable	Value
$\boldsymbol{I}_o$ (kg m^2)	$\begin{bmatrix} 1100 & -20 & -10 \\ -20 & 900 & -15 \\ -10 & -15 & 800 \end{bmatrix}$
$I_{g,i}, I_{s,i}, I_{t,i}$ $(i = 1, 2, \ldots, n)$ (kg m^2)	0.0336, 0.0535, 0.0356
I (kg m^2)	0.0398
$\Omega_{\min}$, $\Omega_{\max}$ (r/min)	3600, 7200
Ω_0 (r/min)	6000
$\dot{\delta}_{\min}$, $\dot{\delta}_{\max}$ ((°)/s)	0.05, 60
$\boldsymbol{\delta}_0$ (°)	$[90, 0, -90, 0]^{\mathrm{T}}$
T_{e1}, T_{e2}, T_{e3} (N m)	0.0002, 0.002, 0.02

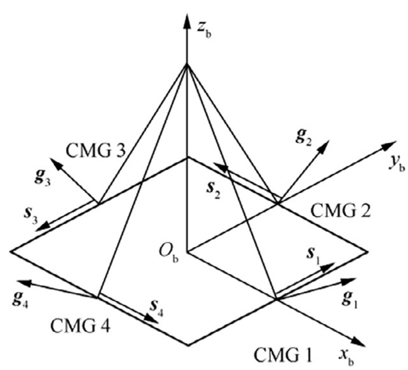

Fig. 3 VSCMG system with standard pyramid configuration.

Pleiades-HR.[5] Assume 4 VSCMGs are mounted in the spacecraft with a standard pyramid configuration, as shown in Fig. 3. In addition, Gaussian distributions are applied for the torque noises of the RW sub-mode, and CMG sub-mode outside and inside of the gimbal dead-zone, with all zero means and standard deviations T_{e1}, T_{e2}, T_{e3}, respectively.

The PD parameters for the controller are chosen as

$$\begin{cases} K_{px} = 77, & K_{dx} = 600 \\ K_{py} = 60, & K_{dy} = 500 \\ K_{pz} = 65, & K_{dz} = 550 \end{cases} \tag{52}$$

Table 2 summarizes the parameters for the steering law.

The results presented in Figs. 4–11 are composed of two parts. The first, an attitude maneuver with initial attitude (45°, 0°, 0°) and expected final attitude (0°, 0°, 0°), is carried out to validate the effectiveness of the steering law for CMG/RW hybrid mode. Fig. 4 plots the singularity measurements κ_1 without (Case 1) and with (Case 2) a null motion. In Case 2, we can see that κ_1 increases from zero rapidly, imply-

Table 2 Control parameters.

Variable	Value
W_{gj} $(j = 1, 2, 3, 4)$	1.0
W_{sj}^0 $(j = 1, 2, 3, 4)$	40.0
ε	5.0
k_N	0.2

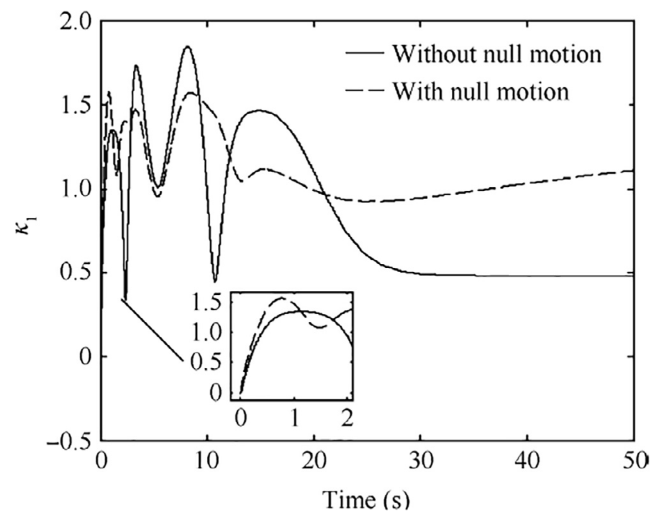

Fig. 4 Singularity measurements κ_1 without and with null motion.

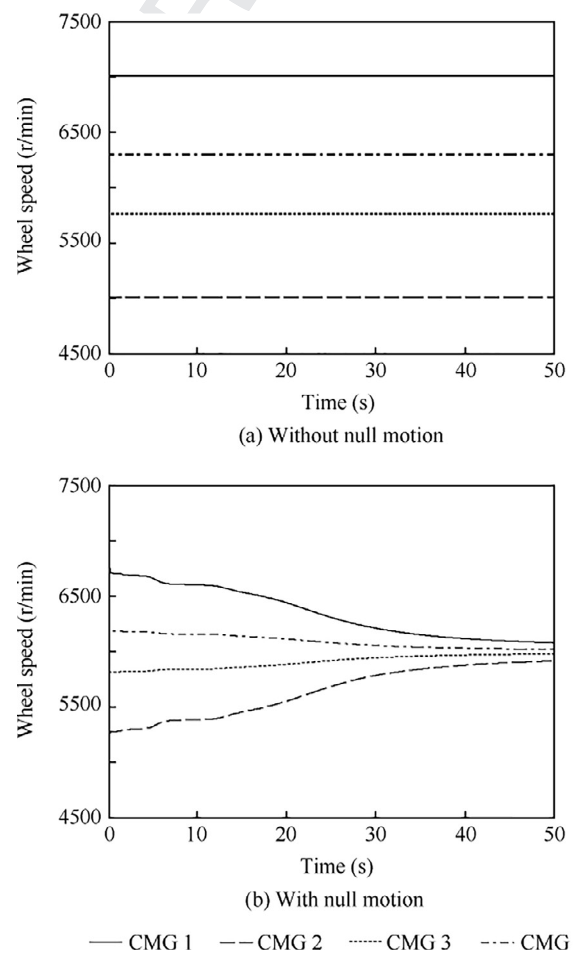

Fig. 5 Wheel speeds without and with null motion.

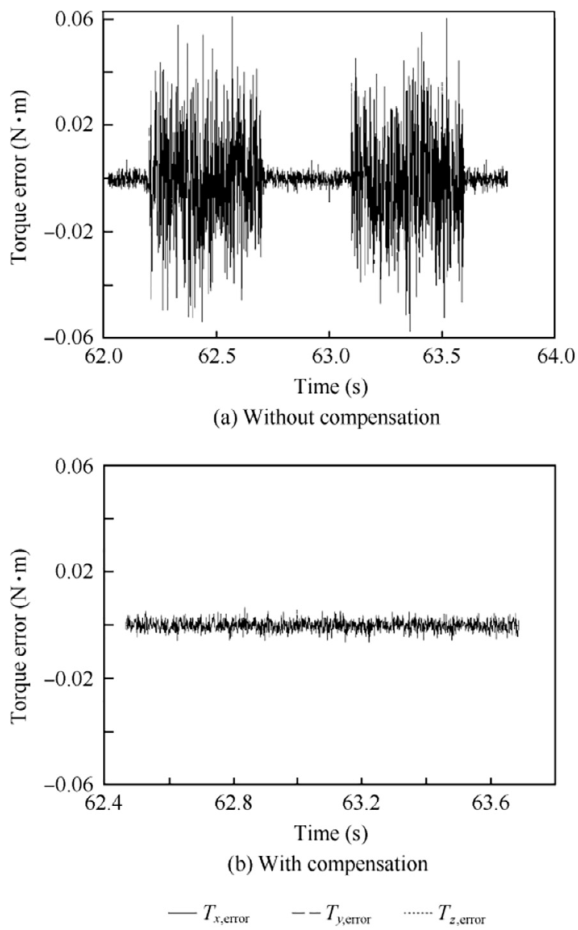

Fig. 6 Torque error without and with compensation of dead-zone nonlinearity.

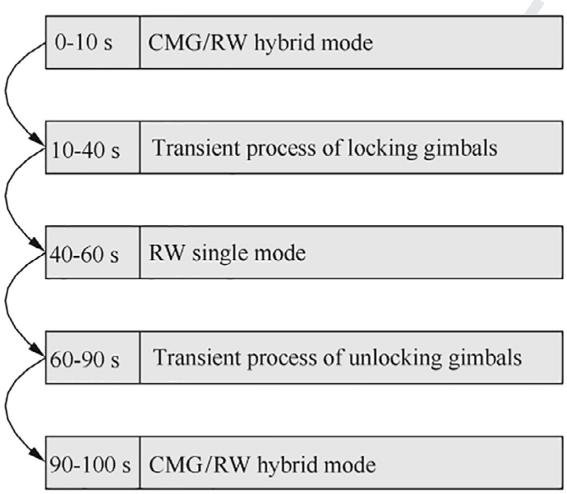

Fig. 7 A typical work cycle.

ing an rapid escape from the initial singular state, and it remains almost always greater than 0.9 afterwards. In contrast, κ_1 can easily become smaller than 0.5 in Case 1. In other words, the gimbal configuration in Case 2 is further away from singular states than that in Case 1. Fig. 5 presents variations of

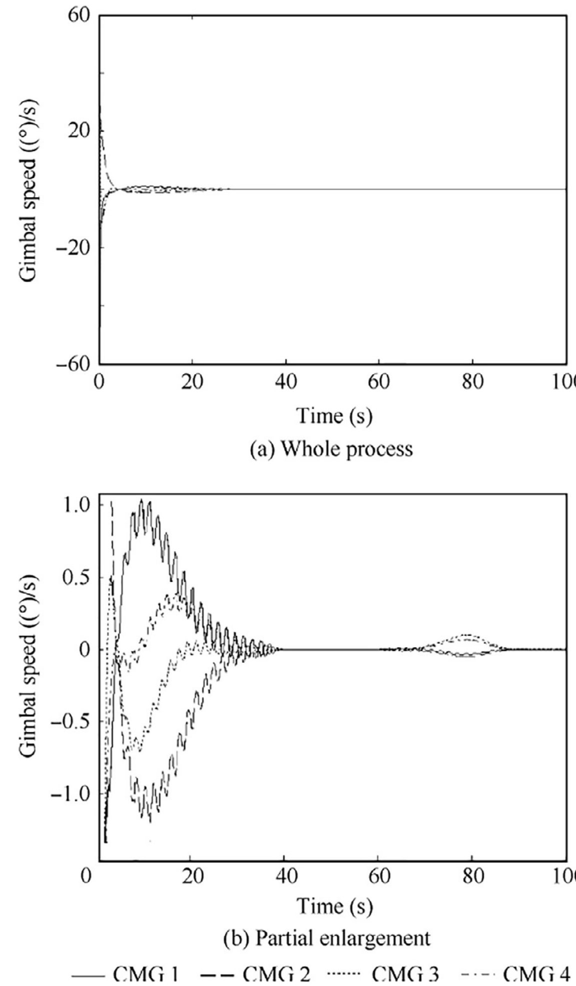

Fig. 8 Gimbal speeds during work cycle.

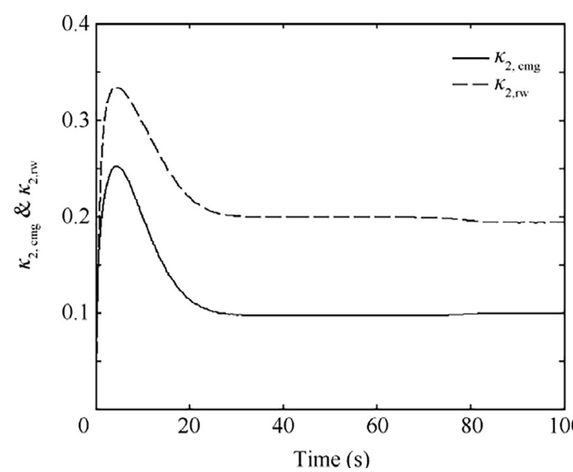

Fig. 9 Singularity measurements of gimbals and wheels during work cycle.

wheel speeds without (Case 1) and with (Case 2) a null motion, and it clearly shows that all wheel speeds tend to approach the desired wheel speed of $\Omega_0 = 6000$ r/min in Case 2, while they almost remain unchanged in Case 1. From these two figures,

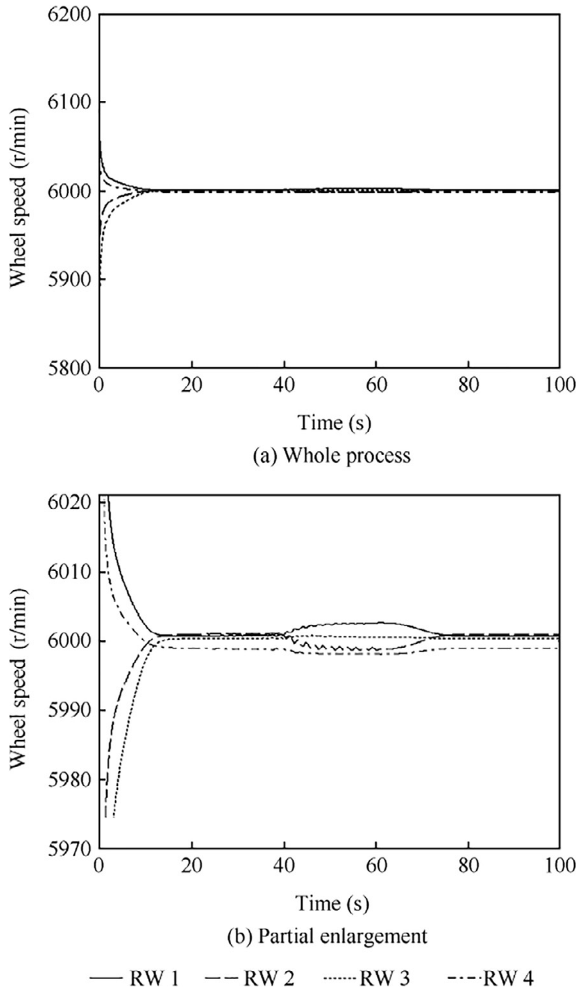

Fig. 10 Wheel speeds during work cycle.

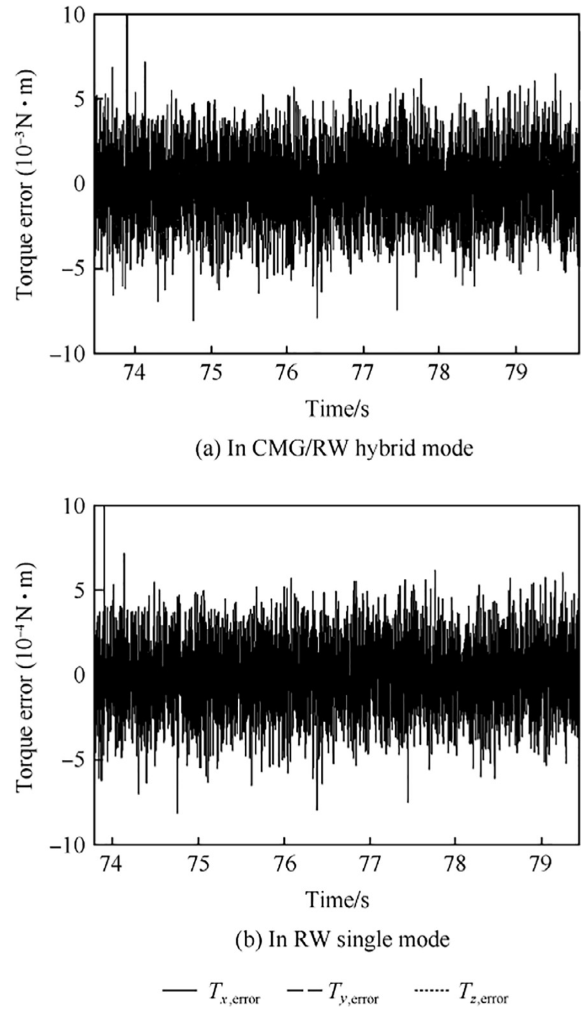

Fig. 11 Torque errors in CMG/RW hybrid mode and RW single mode.

the effectiveness of singularity avoidance/escape and wheel speed equalization via null motion is verified. Fig. 6 compares the torque errors in a time interval of the cases without (Case 1) and with (Case 2) the compensation of the dead-zone nonlinearity. In this time interval, two gimbal speed dead zones appear if no compensation is added. We can see that the torque errors in three axis, $T_{x,error}$, $T_{y,error}$ and $T_{z,error}$, are significantly decreased after the compensation.

In the second part, an attitude stabilization with initial state (1.5°, −1.2°, 0.9°) is implemented to validate the effectiveness of the steering law of RW single mode. VSCMGs go through a typical complete work cycle, as shown in Fig. 7, starting from and eventually getting back to the CMG/RW hybrid mode in the process. Figs. 8–10 show variations in gimbal speeds, the second singularity measurements of the gimbals/wheels, and the wheel speeds during the work cycle. Fig. 8 shows the smoothness of the gimbal speeds in the whole process. Fig. 9 shows that the second singularity measurements of both the gimbals and the wheels are almost always larger than 0.1, implying that constant nonsingular configurations are held for both (once the gimbals or the wheels are near to a singular state, the responding singularity measurement $\kappa_{2,\mathrm{cmg}}$ or $\kappa_{2,\mathrm{rw}}$ will be approximately smaller than 0.05). Fig. 10 shows that the wheel speeds are successfully equalized to the expected speed Ω_0 all the time. These three figures validate the design of the transient processes. Fig. 11 compares torque error of the same small command torque in CMG/RW hybrid mode with compensation of the gimbal speed dead-zone (Case 1, which is not switched into RW single mode) and in RW single mode (Case 2, as in Fig. 7). It shows that the torque error is weakened by one order of magnitude in Case 2, which meets our expectations.

If a singularity is hyperbolic for CSCMGs under a gimbal configuration, the corresponding CMG singularity of VSCMGs under the same gimbal configuration is definitely hyperbolic, since the null motion of CSCMGs is also fit for VSCMGs. Now are two examples showing that elliptic singularities for CSCMGs are still hyperbolic for VSCMGs.

(1) Case 1

For simplicity, unit and all equal magnitude CMG momentum is assumed. The gimbal angles are $\boldsymbol{\delta} = [90^\circ, 0^\circ, -90^\circ, 0^\circ]^{\mathrm{T}}$. The fact $\mathrm{rank}(\boldsymbol{C}) = 2$ demonstrates the singularity of this configuration.

Table 3 Singular type results of an ordinary configuration.

Actuators	Q	eig(Q)	Definite/Indefinite/Singular Q	Singular type
CSCMGs	$\begin{bmatrix} -0.6618 & 1.0174 \\ 1.0174 & -1.6364 \end{bmatrix}$	$\begin{bmatrix} -2.2772 \\ -0.0210 \end{bmatrix}$	Negative definite	Elliptic
VSCMGs	$\begin{bmatrix} -0.6618 & 1.0174 & -0.5024 & 0.5826 & 0.8827 \\ 1.0174 & -1.6364 & 0.5659 & -1.8961 & -0.7322 \\ -0.5024 & 0.5659 & -0.2227 & 0.3389 & 0.3743 \\ 0.5826 & -1.8961 & 0.3389 & -1.2425 & -0.4159 \\ 0.8827 & -0.7322 & 0.3743 & -0.4159 & -0.6614 \end{bmatrix}$	$\begin{bmatrix} -4.3040 \\ -0.9150 \\ 0.5409 \\ 0.2532 \\ 0 \end{bmatrix}$	Infinite and singular	Hyperbolic

For this case, the judgment matrix $\boldsymbol{Q}$ for CSCMGs by Ref. 11 is

$$\boldsymbol{Q}_{\text{CSCMGs}} = \begin{bmatrix} 1.2000 & -0.7200 \\ -0.7200 & 0.8640 \end{bmatrix} \tag{53}$$

and its eigenvalues are

$$\text{eig}(\boldsymbol{Q}_{\text{CSCMGs}}) = [0.2927, 1.7713]^{\text{T}} \tag{54}$$

It is evident that $\boldsymbol{Q}_{\text{CSCMGs}}$ is positive definite and this singularity is elliptic.

On the contrary, in case of VSCMGs, the judgment matrix is

$$\boldsymbol{Q}_{\text{VSCMGs}} = \begin{bmatrix} 1.2000 & -0.7200 & 0.6000 & 0.7200 & -0.6000 \\ -0.7200 & 0.8640 & -2.3867 & -2.8640 & 2.3867 \\ 0.6000 & -2.3867 & 3.3778 & 4.0533 & -3.3778 \\ 0.7200 & -2.8640 & 4.0533 & 4.8640 & -4.0533 \\ -0.6000 & 2.3867 & -3.3778 & -4.0533 & 3.3778 \end{bmatrix} \tag{55}$$

and its eigenvalues are

$$\text{eig}(\boldsymbol{Q}_{\text{VSCMGs}}) = [-0.7727, 0, 0, 1.1120, 13.3443]^{\text{T}} \tag{56}$$

We can see that $\boldsymbol{Q}_{\text{VSCMGs}}$ is indefinite and singular, which leads to a hyperbolic singularity.

(2) Case 2

Generally speaking, one wheel speed of the VSCMGs is not absolutely consistent with another. Therefore, a more general case is presented here, with the CMG momentum magnitudes $[h_1, h_2, h_3, h_4] = [1.0,\ \ 1.25,\ \ 1.2,\ \ 1.5]$ N m s instead of all unit and equal magnitudes, and an ordinary gimbal angle configuration $\boldsymbol{\delta} = [115.0226734945402°, 31.838080532974608°, 151.0592758679665°, -4.953509020906268°]^{\text{T}}$. rank($\boldsymbol{C}$) = 2 indicates the singularity of this configuration. Corresponding results are shown in Table 3. In this case, an elliptic singularity for CSCMGs is hyperbolic for VSCMGs once more.

From these two examples, we can see that the CMG singular type of VSCMGs is hyperbolic while that of CSCMGs is elliptic in a case of the same gimbal angles, and this is in accordance with the conclusion of Theorem 1.

6. Conclusions

(1) In order to achieve high-precision output torque, VSCMGs operation modes are distinguished according to the command torque; the CMG/RW hybrid mode for large command torque and the RW single mode with gimbals locked for small command torque.

(2) The steering law for the CMG/RW hybrid mode covers the problems of torque distribution, singularity avoidance/escape, wheel speed equalization, and compensation of the dead-zone nonlinearity of gimbal speeds. In addition, a theorem and proof illustrate that all internal CMG singularities of VSCMGs are definitely hyperbolic.

(3) Mode switching strategies are realized by the planning of the transient processes for locking or unlocking the gimbals, and the steering law for the RWs with completely locked gimbals is designed by using the pseudo-inverse solution. They comprise the steering law of the RW single mode.

(4) Numerical results validate the effectiveness of the proposed steering law, which allows a set of VSCMGs to meet the requirement of providing both high-precision large and high-precision small torque.

Acknowledgement

This study was supported by the National Natural Science Foundation of China (No. 11272027).

Appendix A

The second singularity measurement of the gimbal structure is defined as

$$\kappa_2 = \frac{\sigma_{3t}}{\sigma_{1t}} \tag{A1}$$

where σ_{1t} and σ_{3t} are the maximum and minimum singular values of $\boldsymbol{A}_t$, respectively. By means of singular value decomposition, $\boldsymbol{A}_t$ is given by

$$\boldsymbol{A}_t = \boldsymbol{U}_t\boldsymbol{S}_t\boldsymbol{V}_t^{\text{T}} = \sum_{i=1}^{3}\sigma_{it}\boldsymbol{u}_{it}\boldsymbol{v}_{it}^{\text{T}} \tag{A2}$$

where σ_{it} ($i = 1, 2, 3$) are the singular values of $\boldsymbol{A}_t$, and $\boldsymbol{u}_{it}$, $\boldsymbol{v}_{it}$ the column vectors of $\boldsymbol{U}_t$ and $\boldsymbol{V}_t$, respectively. Eq. (A2) multiplied by $\boldsymbol{v}_{jt}$ and $\boldsymbol{u}_{jt}$ leads to

$$\boldsymbol{A}_t\boldsymbol{v}_{jt} = \sigma_{jt}\boldsymbol{u}_{jt} \quad j = 1, 2, 3 \tag{A3}$$

$$\boldsymbol{A}_t^{\text{T}}\boldsymbol{u}_{jt} = \sigma_{jt}\boldsymbol{v}_{jt} \quad j = 1, 2, 3 \tag{A4}$$

Calculating $\boldsymbol{u}_{jt}^{\text{T}}\frac{\partial(\text{Eq. (A3)})}{\partial\delta_i} + \boldsymbol{v}_{jt}^{\text{T}}\frac{\partial(\text{Eq. (A3)}}{\partial\delta_i}$ results in

$$\boldsymbol{u}_{jt}^{\mathrm{T}}\frac{\partial \boldsymbol{A}_t}{\partial \delta_i}\boldsymbol{v}_{jt} + \boldsymbol{v}_{jt}^{\mathrm{T}}\frac{\partial \boldsymbol{A}_t^{\mathrm{T}}}{\partial \delta_i}\boldsymbol{u}_{jt} + (\boldsymbol{u}_{jt}^{\mathrm{T}}\boldsymbol{A}_t - \boldsymbol{v}_{jt}^{\mathrm{T}}\sigma_j)\frac{\partial \boldsymbol{v}_{jt}}{\partial \delta_i} + (\boldsymbol{v}_{jt}^{\mathrm{T}}\boldsymbol{A}_t^{\mathrm{T}} - \boldsymbol{u}_{jt}^{\mathrm{T}}\sigma_{jt})\frac{\partial \boldsymbol{u}_{jt}}{\partial \delta_i} = \frac{\partial \sigma_{jt}}{\partial \delta_i}(\boldsymbol{u}_{jt}^{\mathrm{T}}\boldsymbol{u}_{jt} + \boldsymbol{v}_{jt}^{\mathrm{T}}\boldsymbol{v}_{jt}) \tag{A5}$$

This allows for $\frac{\partial \sigma_{jt}}{\partial \delta_i}$ to be expressed as

$$\frac{\partial \sigma_{jt}}{\partial \delta_i} = \frac{1}{2}\left(\boldsymbol{u}_{jt}^{\mathrm{T}}\frac{\partial \boldsymbol{A}_t}{\partial \delta_i}\boldsymbol{v}_{jt} + \boldsymbol{v}_{jt}^{\mathrm{T}}\frac{\partial \boldsymbol{A}_t^{\mathrm{T}}}{\partial \delta_i}\boldsymbol{u}_{jt}\right) = \boldsymbol{u}_{jt}^{\mathrm{T}}\frac{\partial \boldsymbol{A}_t}{\partial \delta_i}\boldsymbol{v}_{jt} \tag{A6}$$

where $\frac{\partial \boldsymbol{A}_t}{\partial \delta_i}$ can be obtained by the δ_i derivative of Eq. (8):

$$\frac{\partial \boldsymbol{A}_t}{\partial \delta_i} = [\boldsymbol{0}_{3\times1}, \boldsymbol{0}_{3\times1}, \ldots, \boldsymbol{0}_{3\times1}, -\boldsymbol{s}_i, \boldsymbol{0}_{3\times1}, \boldsymbol{0}_{3\times1}, \ldots, \boldsymbol{0}_{3\times1}]_{3\times n} \tag{A7}$$

Substituting Eq. (A7) into Eq. (A6), $\frac{\partial \sigma_{jt}}{\partial \delta_i}$ becomes

$$\frac{\partial \sigma_{jt}}{\partial \delta_i} = -\boldsymbol{u}_{jt}^{\mathrm{T}}\boldsymbol{s}_i v_{ij,t} \tag{A8}$$

with the definition $\boldsymbol{v}_{jt}^{\mathrm{T}} = [v_{1j,t}, v_{2j,t}, \ldots, v_{ij,t}, \ldots, v_{nj,t}]^{\mathrm{T}}$.

Based on Eq. (A8), $\frac{\partial \kappa_2}{\partial \delta_i}$ can finally be computed as follows:

$$\frac{\partial \kappa_2}{\partial \delta_i} = \frac{1}{\sigma_{1t}}\cdot\frac{\partial \sigma_{3t}}{\partial \delta_i} - \frac{\sigma_{3t}}{\sigma_{1t}^2}\cdot\frac{\partial \sigma_{1t}}{\partial \delta_i} = -\frac{1}{\sigma_{1t}}\begin{bmatrix}\boldsymbol{u}_{3t}^{\mathrm{T}}\boldsymbol{s}_1 v_{13,t}\\ \boldsymbol{u}_{3t}^{\mathrm{T}}\boldsymbol{s}_2 v_{23,t}\\ \vdots\\ \boldsymbol{u}_{3t}^{\mathrm{T}}\boldsymbol{s}_n v_{n3,t}\end{bmatrix} + \frac{\sigma_{3t}}{\sigma_{1t}^2}\begin{bmatrix}\boldsymbol{u}_{1t}^{\mathrm{T}}\boldsymbol{s}_1 v_{11,t}\\ \boldsymbol{u}_{1t}^{\mathrm{T}}\boldsymbol{s}_2 v_{21,t}\\ \vdots\\ \boldsymbol{u}_{1t}^{\mathrm{T}}\boldsymbol{s}_n v_{n1,t}\end{bmatrix} \quad i = 1, 2, \ldots, n \tag{A9}$$

References

1. O'Connor BJ, Morine LA. A description and the CMG and its application to space vehicle control. Reston: AIAA; 1967. Report No.: AIAA-1967-0589.
2. Kennel HF. Steering law for parallel mounted double-gimbaled control moment gyros-revision A. Washington, DC: Marshall Space Flight Center; 1981. Report No.: NASA TM-82390.
3. Burt RR. International space station control moment gyro failure. *Adv Astronaut Sci* 2003;**113**(1):543–56.
4. Branets VN, Weinberg DM, Verestchagin VP, Danilov-Nitusov VP, Legostayev VP, Platonov VN, et al. Development experience of the attitude control system using single-axis control moment gyros for long-term orbiting space stations. *Acta Astronaut* 1988;**18**(90):91–8.
5. Girouart B, Sebbag I, Lachiver JM. Performances of the Pleiades-HR agile attitude control system. In: Proceedings of the 5th ESA international conference on spacecraft guidance, navigation and control system; 2002 Oct 22–25; Frascati, Italy; 2003. p. 497–500.
6. Somov YI, Butyrin SA, Matrosov VM, Anshakov GP, Antonov VP, Makarov VP, et al. Ultra-precision attitude control of a large low-orbital space telescope. *Control Eng Pract* 1999;**7**(9):1127–42.
7. Yoshikawa T. Steering law for roof type configuration control moment gyro system. *Automatica* 1977;**13**(4):359–68.
8. John EF. A reactive torque control law for gyroscopically controlled space vehicles. Washington, DC: Marshall Space Flight Center; 1973. Report No.: NASA TM X-64790.
9. Roser X, Sghedoni M. Control moment gyroscope (CMG's) and their application in future scientific missions. In: Proceedings of the 3rd ESA international conference on spacecraft guidance, navigation and control systems; 1996 Nov 26–29; Noordwijk, Netherlands; 1997. p. 523–8.
10. Margulies G, Aubrun JN. Geometric theory of single-gimbal control moment gyro system. *J Astronaut Sci* 1978;**26**(2):159–91.
11. Bedrossian NS, Paradiso J, Bergmann EV, Rowell D. Redundant single gimbal control moment gyroscope singularity analysis. *J Guid Control Dyn* 1990;**13**(6):1096–101.
12. Vadali SR, Oh HS, Walker SR. Preferred gimbal angles for single gimbal control moment gyros. *J Guid Control Dyn* 1990;**13**(6):1090–5.
13. Wie B. New singularity escape/avoidance steering logic for control moment gyro systems. Reston: AIAA; 2003. Report No.: AIAA-2003-5659.
14. Tang L. A research on attitude dynamics and control of spacecraft with control moment gyros [dissertation]. Beijing: Beihang University; 2005 [Chinese].
15. Montfort E, Dulot JL. AOCS with magnetic bearing CMG: From failure to recovery. In: Proceeding of the 5th ESA international conference on spacecraft guidance, navigation and control system; 2002 Oct 22-25; Frascati, Italy; 2003. p. 591-4.
16. Sam PL. Precision CMG control for high-accuracy pointing. *J Spacecraft Rockets* 1974;**11**(4):236–40.
17. Luo Q, Li DX, Zhou WY, Jiang JP, Yang G, Wei XS. Dynamic modeling and observation of micro-vibrations generated by a single gimbal control moment gyro. *J Sound Vib* 2013;**332**(19):4496–516.
18. Defendini A, Morand J, Faucheux P, Guay P, Rabejac C, Bangert K, et al. Control moment gyroscope (CMG) solutions for small, agile satellites. In: Proceedings of the 28th Annual AAS rocky mountain guidance and control conference; 2005 Feb 5–9; Breckenridge, Colorado; 2005. p. 51–67.
19. Rybak SC, Lieberman SI, Hartter LL, Gregory RL, Nakashima AK, Kaczynski RF. Achieving ultrahigh accuracy with a body pointing CMG/RW control system. Florida; Reston: AIAA; 1973. Report No.: AIAA-1973-0883.
20. Skelton II CE. *Mixed control moment gyro and momentum wheel attitude control strategies* [dissertation]. VA: Virginia Polytechnic Institute and State University; 2003.
21. Ford KA, Hall CD. Flexible spacecraft reorientations using gimbaled momentum wheels. In: Proceedings of the 1997 AAS/AIAA astrodynamics conference; 1997 Aug 4–7; Sun Valley, Idaho. Reston: AIAA; 1997. p. 1895–913.
22. Schaub H, Vadali SR, Junkins JL. Feedback control law for variable speed control moment gyroscopes. *J Astronaut Sci* 1998;**46**(3):307–28.
23. Yoon H, Tsiotras P. Singularity analysis of variable speed control moment gyros. *J Guid Control Dyn* 2004;**27**(3):374–86.
24. Schaub H, John LJ. CMG singularity avoidance using VSCMG null motion. Reston: AIAA; 1998. Report No.: AIAA-1998-4388.
25. Jia YH. Study on integrated attitude and power control of a spacecraft [dissertation]. Harbin: Harbin Institute of Technology; 2004 [Chinese].
26. DeVon DA, Fuentes RJ, Fausz JL. Closed-loop power tracking for an integrated power and attitude control system using variable speed control moment gyroscopes. Reston: AIAA; 2004. Report No.: AIAA-2004-5130.
27. Yoon H, Tsiotras P. Spacecraft adaptive attitude and power tracking with variable speed control moment gyroscopes. *J Guid Control Dyn* 2002;**25**(6):1081–90.
28. Kim D, MacKunis W, Fitz-Coy N, Dixon WE. Precision integrated power and attitude control system (IPACS) in the presence of dynamic uncertainty. *J Astronaut Sci* 2011;**58**(1):99–120.
29. Malik MSI, Asghar S. Inverse free steering law for small satellite attitude control and power tracking with VSCMGs. *Adv Space Res* 2014;**53**(1):97–109.

Please cite this article in press as: Huang X et al. A new steering approach for VSCMGs with high precision, *Chin J Aeronaut* (2016), http://dx.doi.org/10.1016/j.cja.2016.10.017

Huang Xinghong is a Ph.D. student in the School of Astronautics at Beihang University. His main research interests include spacecraft control and trajectory planning of space manipulators.

Jia Yinghong is an associate professor and M.S. advisor in the School of Astronautics at Beihang University. His main research interest is spacecraft control.

Xu Shijie is a professor and Ph.D. advisor in the School of Astronautics at Beihang University. His main research interests include spacecraft guidance, navigation and control.